Electron solvation dynamics and reactivity in ionic liquids observed by picosecond radiolysis techniques†

James F. Wishart,* Alison M. Funston,‡ Tomasz Szreder,§ Andrew R. Cook and Masao Gohdo

Received 13th April 2011, Accepted 1st June 2011
DOI: 10.1039/c1fd00065a

On time scales of a nanosecond or less, radiolytically-generated excess electrons in ionic liquids undergo solvation processes and reactions that determine all subsequent chemistry and the accumulation of radiolytic damage. Using picosecond pulse radiolysis detection methods, we observed and quantified the solvation response of the electron in 1-methyl-1-butyl-pyrrolidinium bis (trifluoromethylsulfonyl)amide and used it to understand electron scavenging by a typical solute, duroquinone.

Introduction

Over the past decade ionic liquids (ILs) have enjoyed ever-expanding attention for their potential uses as media for advanced devices and chemical processes,[1] as well as a great deal of scientific curiosity into their unusual structures and properties.[2] In contrast to molecular solvents, ionic liquids are composed solely of oppositely-charged ions that, due to structural irregularities and a complex balance of interactions, pack together poorly into low-melting ($\leq$100 °C) solids or, in some cases, never crystallize. Although ionic liquids are such a diverse class of materials that exceptions can be found to every generality used to describe them, they usually possess a wide liquidus range, good conductivity, moderate to high viscosity, low volatility, good combustion resistance, the ability to dissolve a wide range of materials including biopolymers, and oftentimes very wide electrochemical windows. In addition, the ability to substitute anions and cations, and the addition of heteroatom functional groups or perfluorination to the alkyl chains, provides a tremendous capacity to tune the properties of the ionic liquid or IL mixture for a given purpose.

Many useful applications of ionic liquids involving charge transfer reactions, such as the electrochemical conversion of solar energy, fuel cells, batteries, supercapacitors and sensors, take advantage of the properties mentioned above that can make ILs more durable compared to conventional solvents. Other important potential uses of ionic liquids, for example in the electrorefining and plating of metals, and

Chemistry Department, Brookhaven National Laboratory, Upton, NY, 11973, USA. E-mail: wishart@bnl.gov; acook@bnl.gov; mgohdo@bnl.gov; Fax: +1 631 344-5815; Tel: +1 631 344-4327

† Electronic supplementary information (ESI) available. See DOI: 10.1039/c1fd00065a

‡ Present address: School of Chemistry, Monash University, Clayton, Victoria 3800, Australia. Fax: +61 3 9905 4597; Tel: +61 3 9905 6292; E-mail: Alison.Funston@monash.edu

§ Present address: Department of Radiation Chemistry and Technology, Institute of Nuclear Chemistry and Technology, Dorodna 16, 03-195 Warsaw, Poland. Fax: +48 22 811 1532; Tel: +48 22 504 1204; E-mail: t.szreder@ichtj.waw.pl

in the recycling of spent nuclear fuel, necessitate an understanding of their chemistry in contact with extremely reactive species.

Radiation chemistry and pulse radiolysis have been very useful in the study of charge transfer reactions and in characterizing highly reactive species in conventional solvents, so it stands to reason that they would be valuable techniques for studying the same problems in ionic liquids. It is also important to know what will happen when ionic liquids are exposed to ionizing radiation. However, early in the investigations of ionic liquid radiation chemistry it became clear that the unusual properties of ILs have profound impacts that differentiate their radiation-induced chemistry from that of conventional molecular solvents. The largest factor contributing to the difference is the much slower dynamical response of ionic liquids to the motion of charge, due to a number of factors that have been and currently remain the subjects of intense study in the experimental and theoretical physical chemistry communities. Relative to conventional solvents, the relative dynamical slowness of ionic liquids directly alters the physical behavior of a key primary radiolysis product, the excess electron, as depicted in Fig. 1.

An excess electron is created when it is ejected from a molecule during the primary radiolytic event, leaving behind a vacancy, or "hole". The electron thus liberated is "excess" with respect to the solvent, in that it is in addition to the (local) solvent's normal complement of electrons. When it comes to kinetic rest it is called a "dry" or "pre-solvated" electron, because the solvent still has to reorganize in multiple dynamical steps (curved arrows) in response to the sudden appearance of the electron, eventually reaching a "solvated" state. The complete solvation of the excess electron in molecular solvents is extremely rapid at room temperature, occurring in less than a picosecond in water, and on the order of several picoseconds in alcohols, for example, 6.9 ps in ethanol as measured using photoionisation techniques.[4]

In contrast, the dynamical slowness of ILs means that it can take 100 to 1000 times longer for the ionic liquid medium to reach a completely solvated configuration in response to charge redistribution.[5,6] As a result, the excess electrons persist in energetic, weakly trapped, highly mobile and reactive pre-solvated states for a much longer period of time than in conventional solvents, during which time they may react to give products and product distributions quite unlike those resulting from solvated electrons. For example, in Fig. 1 the initially-produced pre-solvated electron has sufficient potential energy to react with scavenger S, but more relaxed, partially or completely solvated electrons would not.

Being highly mobile and reactive, pre-solvated electrons are efficiently scavenged by relatively low concentrations of scavengers that would not be sufficient to scavenge many solvated electrons. This reactivity is significantly more important in ionic liquids because of the much longer lifetimes of pre-solvated electrons in them. Unless taken into account, these facts can lead to unexpected results, as in the case of a pulse radiolysis study on H-atom reactions with pyrene, phenanthrene and other scavengers in the IL methyltributylammonium bis(trifluoromethylsulfonyl)amide,

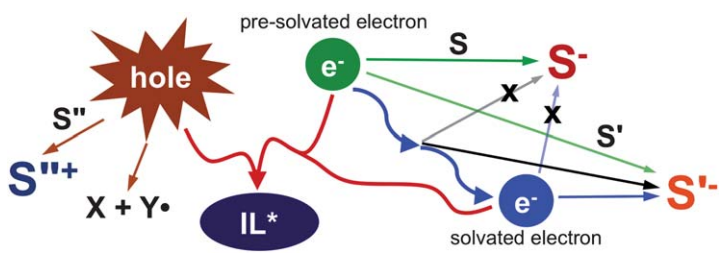

Fig. 1 Reactions of primary radiation-induced species in ionic liquids. S and S′ represent electron scavengers with different reactivity profiles towards solvated and pre-solvated electrons. Adapted with permission from ref. 3. Copyright 2010 American Chemical Society.

$[N_{1444}][NTf_2]$.[7] The experiments were performed by adding acid to the ionic liquid to react with the electrons to form H-atoms, which then react with the arenes to form H-adducts with characteristic spectra (Reactions 1 and 2). The initial work was done with equipment with insufficient time resolution to directly observe the reactions; instead, competition kinetics were used to infer relative rate constant ratios from the product yields.

$$e^-_{solv} + H^+ \rightarrow H^{\cdot} \quad (1)$$

$$H^{\cdot} + \text{pyrene} \rightarrow \text{H-pyrene}^{\cdot} \quad (2)$$

When the reactions were directly observed on faster equipment, the rate constants obtained did not agree with the ratios obtained *via* the competition kinetics. The reason for the product ratio–observed rate constant disparity was the existence of a second pathway to the same H-pyrene$^{\cdot}$ product operating through the direct scavenging of pre-solvated electrons by pyrene, followed by protonation of the pyrene anion (Reactions 3 and 4).

$$e^-_{pre} + \text{pyrene} \rightarrow \text{pyrene}^{\cdot -} \quad (3)$$

$$H^+ + \text{pyrene}^{\cdot -} \rightarrow \text{H-pyrene}^{\cdot} \quad (4)$$

At the pyrene and acid concentrations used, the solvated electron analogue of reaction 3 cannot compete with reaction 1. Therefore, pre-solvated electron reactivity resulted in an unanticipated product distribution in this case.[7] Effects such as this have significant implications for predicting reactivity when IL solutions are exposed to ionizing radiation, as they would be in the recycling of spent nuclear fuel, when undergoing photoionization upon UV exposure, or are subjected to extreme electrochemical conditions as in plasma electrolysis to form metal nanoparticles.[8]

Pre-solvated electron reactivity is usually studied by observing the "missing" fraction of solvated electrons at time zero as the scavenger concentration is increased. An example of this effect is shown in Fig. 2 for increasing concentrations of pyrene in $[N_{1444}][NTf_2]$.

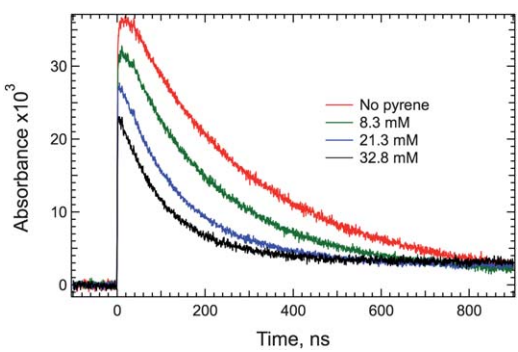

Fig. 2 Absorbance traces of solvated electron decay at 1030 nm for various concentrations of pyrene in $[N_{1444}][NTf_2]$. Adapted with permission from ref. 9. Copyright 2003 American Chemical Society.

The relative yield (absorbance) of solvated electron for a given scavenger concentration is obtained by fitting the observed solvated electron decay kinetics and extrapolating them to time zero. As the pyrene concentration increases, the "initial" concentration of e^-_{solv} drops, which is attributed to scavenging of the solvated electron's precursor e^-_{pre}. This effect is quantified using the relationship $G_c/G_0 = \exp(-c/C_{37})$, where G_c is the yield of solvated electrons at a given scavenger concentration c, G_0 is the yield in the absence of scavenger, and C_{37} is the concentration where only 1/e (37%) of the electrons survive to be solvated.[10] The lower a given scavenger's C_{37}, the more efficient it is at scavenging pre-solvated electrons, and values below 100 mM are considered fairly efficient. Many organic and inorganic scavengers have been rated for their efficiency using this method.[10,11]

However, studying a process by using its effect to make things disappear (such as solvated electrons) can be frustratingly indirect. With our current accelerator technology[12,13] and the larger time window afforded by sluggish ionic liquid dynamics, it is possible to directly observe pre-solvated electrons in ionic liquids and watch them react with solutes. We report here the solvation dynamics of the electron in the ionic liquid 1-methyl-1-butyl-pyrrolidinium bis(trifluoromethylsulfonyl)amide, $[C_4mpyr][NTf_2]$, and observe the reactivity of multiple species of excess electrons with a representative scavenger, duroquinone.

Experimental

Synthesis and materials

The synthesis of the ionic liquids used for the pulse-probe radiolysis studies is reported in the supporting information.† Additional $[C_4mpyr][NTf_2]$ used for the OFSS studies (see below) was purchased from IoLiTec (Tuscaloosa, Alabama, USA).

Instrumentation

Ultraviolet/visible spectra were recorded on an HP 8452A diode array spectrophotometer. ^1H and ^{13}C NMR spectra were measured using a Bruker AVANCE400 spectrometer. The water contents of the samples were measured after each experiment using a Mettler Toledo DL39 Coulometric Karl Fisher Titrator. Microwave syntheses of quaternary pyrrolidinium salts were carried out using a CEM Discover synthesizer.

Pulse radiolysis

Radiolysis experiments were carried out at the Brookhaven National Laboratory Laser-Electron Accelerator Facility (LEAF).[12] Two methods were used to measure transient absorption kinetics on the picosecond time scale. The kinetics of excess electron solvation were followed in the visible and near-infrared using a pulse-probe method, analogous to the laser pump–probe technique, for times up to 10 ns and using fast detectors coupled to a transient digitizer for times longer than 2 ns. The electron pulse width was 9–14 ps in the pulse-probe experiment and <60 ps in the transient digitizer experiment.

In pulse-probe measurements the transient absorbance is determined at a single time delay relative to each accelerator pulse using a dual beam (sample and reference) optical setup, requiring a few thousand pulses to obtain a kinetic trace, using a typical average of 20–50 absorption measurements per delay time and 100–140 delay times in a scan. The detection system for the picosecond pulse-probe measurements is described elsewhere.[12] For these experiments, 30–50 mL of argon-saturated ionic liquid was recirculated through a 10 mm path length cell. The circulation system was kept under a positive pressure of argon to minimize infiltration of air and moisture. Optical probe pulses at wavelengths of 600–1700 nm were generated using

a Quantronix Topas Optical Parametric Amplifier (OPA). Silicon photodiodes (PIN-10D) were used for detection from 400 to 1000 nm and InGsAs photodiodes (PDA400) from 1000 to 1700 nm. Signals were digitized using a LeCroy 9354 oscilloscope in segment mode, triggered at the repetition rate of the laser. The radiolytic dose for each accelerator shot was measured using a Faraday cup and the results used to correct the measured absorbance data point-by-point to the same dose, and used to normalize the absorbance traces for the purpose of spectral analysis. As is standard for such measurements, the delay time interval between data points was varied in steps between 2 ps around time zero to 200 ps after $t = 3$ ns. For the purpose of singular value decomposition (SVD) analysis using Wavemetrics Igor software, absorbance traces at uniform time intervals of 2 ps were created by interpolation of the original data traces with irregular time intervals and then assembled into a matrix of absorbance values *vs.* wavelength and time for the SVD procedures.

Subsequently, an "Optical Fiber Single-Shot" (OFSS) detection method was developed at the LEAF facility for picosecond time-resolved pulse radiolysis experiments on samples that cannot be flowed or are limited in quantity.[13] The OFSS system uses a bundle of optical fibers, each of different length, to divide a laser probe pulse into a multiplexed spatial array of 143 varied delay times over a span of 5 nanoseconds, with intervals of ~5 ps around time zero. The image of the fiber bundle output is split and transported along a reference arm to a CCD camera and through the irradiated region of the sample to another CCD camera. The integrated light intensities for each fiber are used to calculate an absorbance for the time corresponding to the calibrated delay of the fiber, thus creating an absorbance *vs.* time trace in a single shot, although the data is usually averaged for 25–64 shots for a better signal-to-noise ratio. The OFSS method is superior to the pulse-probe method in terms of damage incurred by the sample (~100-fold less) and acquisition time, but presently it is only available for wavelengths <1000 nm because we have yet to acquire NIR-sensitive area detectors. Consequently, OFSS is not yet available in the region best suited to observe pre-solvated electrons. Samples for OFSS experiments were placed in 5 mm path length Suprasil spectrophotometer cuvettes fitted with valves or septum screw caps and prepared as described below for nanosecond measurements.

The excellent mutual agreement of the pulse-probe and OFSS radiolysis detection techniques is shown in supporting information Fig. 1S,† where kinetic data on the radiolysis of neat, argon-saturated [C_4mpyr][NTf_2] measured at 800 and 900 nm by both techniques are superimposed. The data were collected on IL samples of different provenance.

For nanosecond experiments the electron pulse was focused into a spectrophotometer cell containing the solution of interest. The monitoring light source was a 75 W xenon arc lamp pulsed to a few hundred times its normal intensity, propagating colinearly with the electron beam but in the opposite direction so as to minimize collection of Cerenkov radiation emitted within the sample by the passage of the electron bunch. Wavelengths were selected using either 40 nm or 10 nm bandpass optical interference filters. Transient absorption signals were detected with either an FND-100Q silicon diode (≤1000 nm) or a GAP-500L InGaAs diode (1100–1700 nm) and digitized using Tektronix TDS-680B, Tektronix TDS-694C or LeCroy 8620A oscilloscopes. Absorption spectra were corrected for the secondary response distortion from the NIR detector[14] by normalization of the signal at time t to the signal from the FND100Q silicon diode at the same time and wavelength. The total dose per pulse was determined before each series of experiments using an N_2O-saturated solution of aqueous 10 mM KSCN where $G\varepsilon = 4.87 \times 10^4$ ions $(100\ \text{eV})^{-1}\ \text{M}^{-1}\ \text{cm}^{-1}$ for the $(SCN)_2^-$ radical at 472 nm. Radiolytic doses of 15–35 Gy, corrected for electron density, were used. The absorption *vs.* time data were analysed with Igor Pro software (Wavemetrics).

The ionic liquids were dried overnight in a vacuum oven at 40 °C immediately prior to use. For nanosecond measurements, the liquids were placed in

septum-capped, self-masking semi-micro Suprasil spectrophotometer cuvettes (optical path length 10 mm) and purged by bubbling with argon for at least twenty minutes. During the irradiation experiments the samples were exposed to as little UV light as possible (*via* the use of UV cutoff filters) to avoid photodecomposition; no evidence of this occurring was found within the time frames monitored. Unless stated otherwise, all measurements were performed at 21 ± 1 °C.

Results and discussion

Observation of pre-solvated electrons and their solvation process

Fig. 3 depicts the transient absorption pulse-probe traces for the radiolysis of neat $[C_4mpyr][NTf_2]$, recorded at 100 nm intervals from 600 nm to 1600 nm. Unfortunately, data could not be collected at 1100 nm due to weak OPA output and at 1200 nm due to strong sample background absorption. The traces taken at 1400–1600 nm show a quick absorbance decrease over the first few hundred picoseconds, while the traces from 800–1000 nm show an increase over the same interval. On this time scale there is clearly a blue shift of the absorption feature assigned to the radiolytically-generated excess electrons.

The blue shift is more apparent if the kinetic traces are sliced into spectra at selected time intervals as shown in Fig. 4. To guide the eye, the discrete absorption data for each spectral slice have been fitted with a spline curve. The spectra can be compared with the spectrum of the solvated electron at 50 ns after the radiolysis pulse, obtained using the standard transient digitizer pulse radiolysis technique, also included in Fig. 4. The species responsible for this absorption on the longer time scale (≥2 ns) has been unambiguously assigned as the solvated electron based on its spectrum and reactivity in this and other ionic liquids[9,15] and by analogy to red- and NIR-absorbing solvated electrons observed in conventional solvents.[16] The prominent absorption feature on the red side of the early-time spectra is thus reasonably attributed to excess electrons that have not yet reached their equilibrium solvation state, a population of pre-solvated electrons. However, due to the limited time resolution of the pulse-probe radiolysis experiment it is likely that the observed NIR absorption does not correspond to the "driest" form of the pre-solvated electron (green circle in Fig. 1), which would absorb even further in the NIR, but rather to an intermediate, probably penultimate, state of solvation.

It can be seen from the long-wavelength decay kinetics in Fig. 3 and the spectra in Fig. 4 that the relaxation of the excess electron to its equilibrated solvation state is

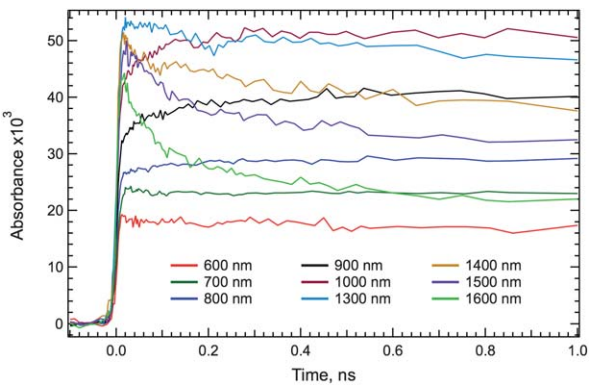

Fig. 3 The first nanosecond of the time-resolved pulse-probe pulse radiolysis transient absorption traces for neat $[C_4mpyr][NTf_2]$ under argon atmosphere at the wavelengths indicated in the legend. The entire 8.2 ns range collected is shown in supporting information Fig. 2S.†

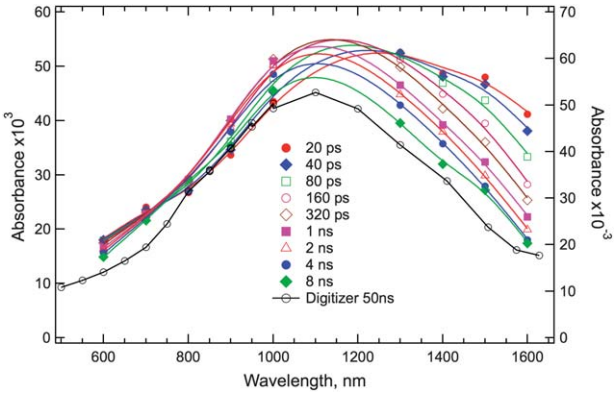

Fig. 4 Transient absorption spectra constructed by taking slices at indicated delay times from the pulse-probe radiolysis data in Fig. 3 for [C_4mpyr][NTf_2] under argon atmosphere (left axis). For comparison, the spectrum of the solvated electron in [C_4mpyr][NTf_2] at 50 ns, constructed from digitized transients using an oscilloscope and Si and InGaAs photodiodes, is included and scaled for visibility (right axis).

complete within one nanosecond. Except for the shifted peak wavelengths of the electron spectra, the results resemble in shape and time scale those obtained by Zhang and Jonah in cold (−30 °C) propanol using a stroboscopic radiolysis technique,[17] and even earlier work by Baxendale and Wardman.[18] The 50-degree difference in working temperatures attests to the effect of slower dynamics in ILs.

In order to quantify the observed spectral shift related to the solvation process, singular-value decomposition (SVD) was applied to the absorbance-time data over all wavelengths. Using SVD, the matrix of absorbance values *vs.* *m* time points and *n* wavelengths, A_{mn}, can be broken down into the product of three matrices—an orthogonal matrix U_{mn} containing signal amplitude *vs.* time vectors, a diagonal matrix S_{nn} containing the singular values, and the transpose of an orthogonal matrix V^T_{nn} containing the absorbance spectral vectors:

$$A_{mn} = U_{mn}\, S_{nn}\, V^T_{nn} \tag{5}$$

When SVD is applied to the data in Fig. 3 (over the entire 8.2 ns time range), the diagonals of the singular value matrix *S* are (6.332, 0.250, 0.075, 0.054, 0.043, 0.037, 0.032, 0.026, 0.014). Considering the distribution of the singular values, it is reasonable to consider only the first two vectors of the *U* and V^T matrices as meaningful and all the rest as dominated by noise. To test this assumption, the absorbance data matrix *A* was reconstructed using only the first two singular values and plotted against the original data (see supporting information Fig. 3S†). The reconstructed traces coincide well with the original data except for slightly under-predicting the absorbance at 700 and 800 nm at times below 150 ps. This discrepancy is not significant for the analysis.

As shown in Fig. 5, the elements that dominate the SVD analysis of the pulse-probe data consist of the $n = 0$ spectrum and slow decay kinetics (in green) that correspond to the solvated electron, as evidenced by the excellent agreement between the $n = 0$ spectrum and that of the solvated electron at 50 ns (blue dotted line) in the inset. The general shape of the solvated electron decay represented by U_{m0} is consistent with geminate recombination processes typically seen in pulse radiolysis. The amplitude of the $n = 0$ signal corresponding to the solvated electron at time zero (with respect to the ~15 ps resolution of our experiment) indicates that a large component of the relaxation of the initially dry and delocalized excess electrons occurs in less than 15 picoseconds. A dual channel mechanism, invoking direct

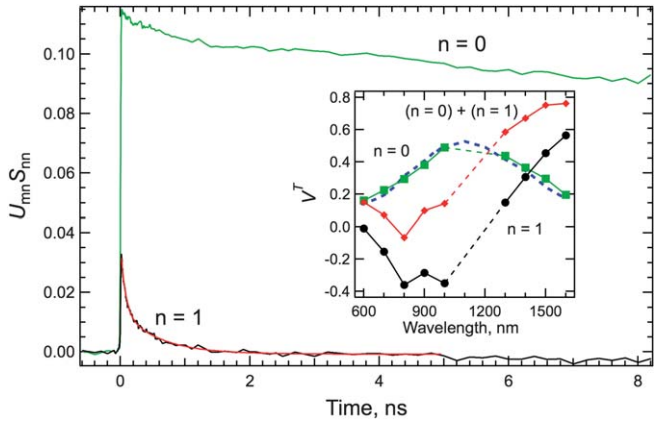

Fig. 5 SVD results for the pulse probe radiolysis of neat [C_4mpyr][NTf_2]. In the larger graph, the signal amplitudes *vs.* time $U_{m(n=0,1)}$ are multiplied by their corresponding singular values S_{00} and S_{11}. A double-exponential fit to the $n = 1$ vector for the first 5 ns is shown in red. The inset shows the spectral vectors corresponding to the first two singular values and their sum (red trace). The dotted blue line is the measured absorption spectrum of the solvated electron at 50 ns (as in Fig. 4) scaled to coincide with the zero-order spectral vector.

relaxation of delocalized excess electrons into solvated states in addition to the stepwise process, has been postulated in the radiolysis of alcohols.[19,20] In Fig. 1, this corresponds to a direct path from the green electron at the top to the blue one at the bottom. It is also known that in spite of the general slow relaxation of ionic liquids there are dynamical components, often characterized as inertial, that occur on femtosecond and sub-10-picosecond time scales that could facilitate this direct relaxation process.[5,21]

Despite the prevalence of the direct or fast pathways for solvated electron formation, the $n = 1$ vectors correspond to the solvation process of a penultimate form of pre-solvated electron. Lewis and Jonah[19] called this species the trapped electron, e^-_{tr}. If the $n = 1$ spectrum corresponds to the difference between the pre-solvated and solvated electron spectra, the sum of the two vectors, depicted in red in the inset and apparently peaking around 1500–1600 nm, must correspond to the spectrum of e^-_{tr}. The size and position of this band is consistent with similar spectra obtained in methanol by Keszei and coworkers[20] when allowance is made for the difference in solvated electron peak position in methanol *vs.* this ionic liquid. In both cases the peak of e^-_{tr} is shifted about 2500 cm^{-1} to the red compared to e^-_{solv}.

Turning our attention to the kinetics of the e^-_{tr} solvation process represented by the $n = 1$ signal vector, the average solvation time obtained by integrating the transient curve is 270 ps. The response fits well to a double exponential with time constants of 70.4 and 574 ps and amplitudes of 60% and 40%, respectively, as indicated by the red curve in Fig. 5. Both exponential terms are associated with the same spectral change. They represent yet another case of distributed, stretched- or multi-exponential kinetics observed in ionic liquids often attributed to their distribution of heterogeneous local environments.[5,22] However, distributed kinetics can also occur in homogeneous environments, particularly when relaxation phenomena are involved.[23]

It is reasonable to wonder how the solvation dynamics of e^-_{tr} in [C_4mpyr][NTf_2] compare with those of the popular solvatochromic fluorescent coumarin dye C153 in the same solvent, which has been investigated by several groups. Because many different methods are used to characterize the correlation functions that are typically constructed from fluorescence emission peak frequencies, it is easiest to compare the reported average C153 solvation times with the value of 270 ps obtained here for the electron at 21 °C. Jin *et al.*[6] obtained 380 ps at 25 °C ($\eta = 70$ cP), Funston *et al.*[24]

obtained 346 ps at 20 °C ($\eta = 95$ cP) and Mandal and Samanta[25] obtained 500 ps at 25 °C ($\eta = 70$ cP). It must be noted that the operative assumption in the treatment of fluorescence Stokes shifts as solvation dynamics probes is that the shift is continuous, while we have treated the electron solvation as a state-to-state transition using the SVD approach. For comparison, we constructed a correlation function for the electron spectral shift as a continuous process using the same methods employed in ref. 24 by fitting spectra at time intervals and plotting the peak frequencies. The results are presented in the supporting information (Fig. 4S†). The correlation function thus obtained indicates a substantially faster response than the SVD model, with an average solvation time of 113 ps and fitting to a double exponential function with time constants of 35 (62%) and 200 ps (38%). Recently, Bonin *et al.*[26] examined electron solvation in hot glycerol (60 °C, $\eta = 76$ cP) and found that the dynamics could be modelled well either by a stepwise mechanism involving two species or a continuous relaxation one with biexponential functions, although the time constants for glycerol were over ten times shorter than observed here for an IL of similar bulk viscosity.

One might also ask what similarities to expect between the ionic liquid relaxation processes for solvation of e^-_{tr} and dipole reorientation in the case of solvatochromic dyes. It is likely that the two processes interrogate a different profile of response dynamics, but concrete answers must await detailed quantum MD simulations on electron solvation in ILs before comparisons can be made. When available, these simulations may also provide guidance as to whether the continuous or state-to-state transition model is most appropriate.

Pre-solvated electron scavenging by duroquinone in [C_4mpyr][NTf_2]

One of the primary motivations for studying electron solvation processes in ionic liquids is to understand how they control pre-solvated electron scavenging reactions, which are of extreme relevance to many important IL applications as laid out in the introduction. We will examine the case of duroquinone (2,3,5,6-tetramethyl-1,4-benzoquinone, DQ) as an electron scavenger in [C_4mpyr][NTf_2] because it illustrates some interesting features relating to the electron solvation process.

As shown in Fig. 6, when the concentration of duroquinone is increased the initial rise in absorbance at 800 nm due to the solvation process disappears and is replaced by an increasingly large fast decay component. (On longer timescales, e^-_{solv} is scavenged by DQ with a rate constant of $(8.6 \pm 0.3) \times 10^8$ M^{-1} s^{-1}.) If the absorbance decays at each DQ concentration are fitted to two exponentials, the rate constant

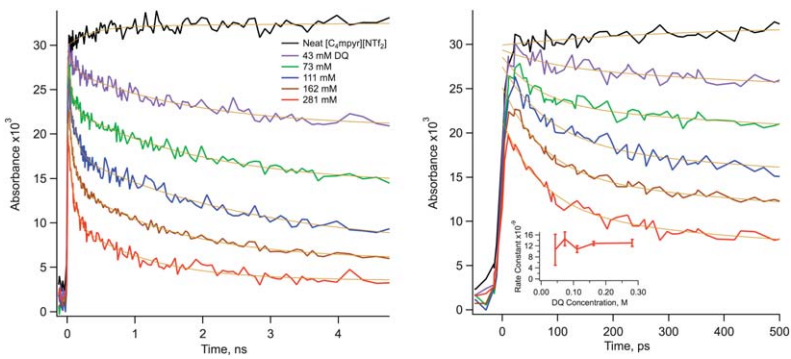

Fig. 6 OFSS transient absorption data at 800 nm in argon-purged [C_4mpyr][NTf_2] with several concentrations of duroquinone (DQ) as indicated in the figure legend (left) and expanded view of the first 500 ps (right). DQ^- anion does not absorb appreciably at this wavelength. Inset on right: the faster of the two rate constants used to fit the absorbance decay plotted against DQ concentration, with error bars representing one standard deviation.

of the fast step does not show any concentration dependence. The corresponding time constant is 76 ps at the highest DQ concentration, effectively the same as the 70 ps fast component of the solvation response function obtained from SVD. Fig. 5S† of the supporting information plots the kinetics of the electron solvation process, electron scavenging at 800 nm by 162 and 281 mM DQ, and the raw pulse-probe absorbance data taken at 1600 nm together on one graph to emphasize that the scavenging decay process coincides with the solvation process.

At first glance it appears odd that the rate of the electron absorbance decay due to scavenging remains constant with increasing scavenger concentration even as the decay increases in amplitude, but it is important to recall that very little diffusion occurs on this time scale in [C_4mpyr][NTf_2]. One explanation for these observations is that true to its name, e^-_{tr} is trapped and its diffusion is restricted, but being in a more energetic state than a solvated electron it is more likely to tunnel to a quencher if one is nearby,[27] and increasing the DQ concentration increases the density of quenchers, resulting in a higher proportion of quenching (absorbance decay at 800 nm) at the expense of solvated electron production.

Compared to the time-zero distribution between e^-_{tr} and e^-_{solv} implied by Fig. 5 it appears that there is a large fraction of e^-_{solv} missing in Fig. 6 at higher [DQ]. This is due to the reaction of DQ with the energetic electron precursor state that produces e^-_{solv} directly without passing through e^-_{tr}. It is also worthwhile to point out that according to the standard C_{37} approach to quantifying pre-solvated electron reactivity, the fast process shown in Fig. 6 would not even be observed and the C_{37} would have been calculated on the basis of the absorbances measured at 4 nanoseconds. The existence of earlier processes would be unknown.

DQ shows one type of reactivity pattern with respect to the various types of excess electron species, but there are many others. Nitrate anion, for example, efficiently targets the production of e^-_{tr} by reacting with its precursor, without strongly affecting the direct production of e^-_{solv} from higher states. Because of the importance of pre-solvated electron scavenging to radiation chemistry in general, and in particular the use of kinetic clocks to explore early events in radiolysis (by increasing scavenger concentrations [S] to push the scavenging power k_S[S] to very short times), a lot of effort has gone into detailing the reactivity profiles of many quenchers.[11,28] Due to their slower dynamical responses, ionic liquids afford luxurious amounts of time (*i.e.* nanoseconds) in which to probe the mechanistic details of scavenging processes. As shown in the example just above, this allows us to conveniently see a wealth of mechanistic detail heretofore much more difficult to observe.

Conclusions

The experiments described here confirm, as has been demonstrated in other cases, that dynamical processes and reactions proceed by similar mechanisms in ionic liquids than they do in conventional solvents, but also that the unusual properties of ionic liquids provide additional wrinkles that enable new insights and opportunities for new science and new technologies. In the case of ionic liquid radiation chemistry, understanding very early electron solvation and scavenging processes will enable us to control the chemistry of primary radiolytic species and direct that reactivity towards intended products and away from undesirable ones. In practical terms, this can improve the radiolytic synthesis of nanoparticles, control photo- and electrochemical degradation of solar cells, display devices and batteries, and minimize the deleterious effects of radiation on spent nuclear fuel recycling processes.

Acknowledgements

This work, and use of the LEAF Facility of the BNL Accelerator Center for Energy Research, was supported by the US Department of Energy, Office of Basic Energy

Sciences, Division of Chemical Sciences, Geosciences, and Biosciences under contract # DE-AC02-98CH10886.

Notes and references

1 J. F. Wishart, *Energy Environ. Sci.*, 2009, **2**, 956–961; N. V. Plechkova and K. R. Seddon, *Chem. Soc. Rev.*, 2008, **37**, 123–150; W. L. Hough and R. D. Rogers, *Bull. Chem. Soc. Jpn.*, 2007, **80**, 2262–2269.
2 J. F. Wishart and E. W. Castner, *J. Phys. Chem. B*, 2007, **111**, 4639–4640; R. D. Rogers and G. A. Voth, *Acc. Chem. Res.*, 2007, **40**, 1077–1078; F. Endres, *Phys. Chem. Chem. Phys.*, 2010, **12**, 1648–1648; D. R. MacFarlane and K. R. Seddon, *Aust. J. Chem.*, 2007, **60**, 3–5; H. Weingartner, *Angew. Chem., Int. Ed.*, 2008, **47**, 654–670.
3 J. F. Wishart, *J. Phys. Chem. Lett.*, 2010, **1**, 3225–3231.
4 P. K. Walhout and P. F. Barbara, in *Ultrafast Processes in Chemistry and Photobiology*, ed. M. A. El-Sayed, I. Tanaka and Y. Molin, Blackwell Scientific, Oxford (England), Cambridge, Massachusetts, 1995, pp. 83–104.
5 A. Samanta, *J. Phys. Chem. Lett.*, 2010, **1**, 1557–1562.
6 H. Jin, G. A. Baker, S. Arzhantsev, J. Dong and M. Maroncelli, *J. Phys. Chem. B*, 2007, **111**, 7291–7302.
7 J. Grodkowski, P. Neta and J. F. Wishart, *J. Phys. Chem. A*, 2003, **107**, 9794–9799.
8 A. Keppler, M. Himmerlich, T. Ikari, M. Marschewski, E. Pachomow, O. Hofft, W. Maus-Friedrichs, F. Endres and S. Krischok, *Phys. Chem. Chem. Phys.*, 2011, **13**, 1174–1181; N. Kulbe, O. Hofft, A. Ulbrich, S. Z. El Abedin, S. Krischok, J. Janek, M. Polleth and F. Endres, *Plasma Process. Polym.*, 2011, **8**, 32–37.
9 J. F. Wishart and P. Neta, *J. Phys. Chem. B*, 2003, **107**, 7261–7267.
10 R. K. Wolff, M. J. Bronskill and J. W. Hunt, *J. Chem. Phys.*, 1970, **53**, 4211–4215; J. E. Aldrich, M. J. Bronskill, R. K. Wolff and J. W. Hunt, *J. Chem. Phys.*, 1971, **55**, 530–539; K. Y. Lam and J. W. Hunt, *Int. J. Radiat. Phys. Chem.*, 1975, **7**, 317–338.
11 C. D. Jonah, J. R. Miller and M. S. Matheson, *J. Phys. Chem.*, 1977, **81**, 1618–1622.
12 J. F. Wishart, in *Radiation Chemistry: Present Status and Future Trends*, ed. C. D. Jonah and B. S. M. Rao, Elsevier Science, Amsterdam, 2001, pp. 21–35; J. F. Wishart, A. R. Cook and J. R. Miller, *Rev. Sci. Instrum.*, 2004, **75**, 4359–4366.
13 A. R. Cook and Y. Z. Shen, *Rev. Sci. Instrum.*, 2009, **80**, 073106.
14 J. A. Cline, C. D. Jonah and D. M. Bartels, *Rev. Sci. Instrum.*, 2002, **73**, 3908–3915.
15 A. M. Funston and J. F. Wishart, in *Ionic Liquids IIIA: Fundamentals, Progress, Challenges and Opportunities*, ed. R. D. Rogers and K. R. Seddon, American Chemical Society, New York, 2005, pp. 102–116; K. Takahashi, T. Sato, Y. Katsumura, J. Yang, T. Kondoh, Y. Yoshida and R. Katoh, *Radiat. Phys. Chem.*, 2008, **77**, 1239–1243.
16 L. M. Dorfman and J. F. Galvas, in *Radiation Research. Biomedical, Chemical and Physical Perspectives*, ed. O. F. Nygaard, H. J. Adler and W. K. Sinclair, Academic Press, New York, 1975, pp. 326–332.
17 X. J. Zhang and C. D. Jonah, *Chem. Phys. Lett.*, 1996, **262**, 649–655.
18 J. H. Baxendale and P. Wardman, *J. Chem. Soc., Faraday Trans. 1*, 1973, **69**, 584–594.
19 M. A. Lewis and C. D. Jonah, *J. Phys. Chem.*, 1986, **90**, 5367–5372.
20 P. Holpar, T. Megyes and E. Keszei, *Radiat. Phys. Chem.*, 1999, **55**, 573–577.
21 S. Arzhantsev, H. Jin, G. A. Baker and M. Maroncelli, *J. Phys. Chem. B*, 2007, **111**, 4978–4989; S. Arzhantsev, H. Jin, N. Ito and M. Maroncelli, *Chem. Phys. Lett.*, 2006, **417**, 524–529.
22 Z. H. Hu and C. J. Margulis, *Proc. Natl. Acad. Sci. U. S. A.*, 2006, **103**, 831–836.
23 C. Khurmi and M. A. Berg, *J. Phys. Chem. Lett.*, 2010, **1**, 161–164.
24 A. M. Funston, T. A. Fadeeva, J. F. Wishart and E. W. Castner, *J. Phys. Chem. B*, 2007, **111**, 4963–4977.
25 P. K. Mandal and A. Samanta, *J. Phys. Chem. B*, 2005, **109**, 15172–15177.
26 J. Bonin, I. Lampre, P. Pernot and M. Mostafavi, *J. Phys. Chem. A*, 2008, **112**, 1880–1886.
27 J. R. Miller, *J. Chem. Phys.*, 1972, **56**, 5173–5183.
28 B. Pastina and J. A. LaVerne, *J. Phys. Chem. A*, 1998, **103**, 209–212; S. M. Pimblott and J. A. LaVerne, *J. Phys. Chem. A*, 1998, **102**, 2967–2975.